Egyptian Journal of Chemistry

http://ejchem.journals.ekb.eg/

Multifunctional Textile Coatings Using Chitosan, Clay, and Metal Oxide Nanoparticles

Asmaa H. Zydan [a], Abdel Monem Fouda [a], and Sahar Shaarawy [b*]

[a] Textile Engineering Department Faculty of Engineering, Mansoura University, 33516, Egypt
[b] Pre-treatment and Finishing of Cellulosic-based Fabric Department, Textile Research and Technology Institute, National Research Center, 33 El-Buhoth St, Dokki, Cairo 12311, Egypt

In Loving Memory of Late Professor Doctor ""Mohamed Refaat Hussein Mahran""

Abstract

Textile fabrics present a promising platform for functionalization due to their integral advantages like adaptability, high surface area, and performance. This work studies the utilization of natural biopolymers and inorganic nanoparticles for surface modification and coating of textile fabrics to provide treated fabrics with multi-functional properties such as antimicrobial, UV blocking, stain repellent, and flame-retardant properties. This work focuses specifically on the use of chitosan as a natural biopolymer, with three different nanoparticles, namely clay, zinc oxide (ZnO), and titanium dioxide (TiO_2) composites, used as coating agents. This study investigates the multi advantages added via chitosan, due to its biocompatibility, biodegradability, nontoxicity, and intrinsic antimicrobial activity. Moreover, it explores the synergistic effect of combining chitosan with nanoparticles, demonstrating enhanced functionalities like improved mechanical stability, flame retardancy, broad spectrum antimicrobial activity, self-cleaning facilities, and UV protection. The study also studies into various coating techniques like dip coating, padding, layer-by-layer assembly, and ultrasonic irradiation, emphasizing their efficacy in achieving sustainable functional chitosan-clay, chitosan-ZnO, and chitosan TiO_2 coatings on textiles. Finally, nanoparticle concentrations are studied in detail to determine the optimum conditions recommended for developing next-generation textiles with multi-optimistic functions based on green, natural materials and accessible fabrication processes.

Keywords: properties, cotton fabric, nano-titanium finishing, nano-clay finishing, nano-zinc finishing, antimicrobial activity, self-cleaning facility and UV protection

1. Introduction

Textile fabrics offer an excellent platform for functionalization due to their versatility, high surface area, and scalability. Through surface modification and coatings, fabrics can be equipped with valuable properties such as antimicrobial, UV blocking, stain repellent and flame-retardant functions. The use of natural biopolymers and inorganic nanoparticles for fabric treatments imparts advantages both in terms of function and sustainability. Chitosan, a natural biopolymer, along with clay, zinc oxide (ZnO), and titanium dioxide (TiO2) nanoparticles, have proven to serve as effective materials for fabric functionalization via robust coating techniques [1-3].

Desirable properties are imparted to cellulosic textile fabrics when they are treated with 3-chloro-2-hydroxypropyl trimethyl ammonium chloride (Quat-188), rendering the fabrics cationic in nature [1] The reaction mechanism as well as reaction efficiency have recently been studied [2]. The quaternary ammonium group $-\oplus N(CH3)4$ has a very high positive charge and can thereby lead to the formation of ionic bonds (salt linkages) with negatively charged anionic groups, such as those found in a wide array of anionic dye classes or compounds containing carboxyl. which impart ionic crosslinking for cotton fabric, giving the fabric the property of wrinkle recovery [2]. Moreover, the presence of cationized groups in the cellulose also impart antimicrobial properties to cotton fabric [3]

Nanoparticles like titanium dioxide (TiO_2) and zinc oxide (ZnO) have been incorporated into textile fabrics to impart self-cleaning properties [4, 5]. These metal oxide nanoparticles create a photocatalytic effect on fabric surfaces. Upon exposure to UV light, the nanoparticles generate reactive oxygen species that can degrade organic matter. This allows the fabric to break down stains and dirt through a photocatalytic process triggered by sunlight. In addition, nano clays can be integrated into fabric coatings. The clay acts as a carrier and delivery system for the TiO_2 and ZnO nanoparticles. The nanoparticle-clay coating also makes the fabric

hydrophobic, so liquids bead up and roll off the surface, carrying away contaminants [6-8]. The combined self-cleaning effect of the metal oxide nanoparticles and nano clays reduces the need for harsh chemical cleaners. With just exposure to light, the treated textiles stay cleaner for longer. The eco-friendly nanoparticle-clay treatment has promising applications for outdoor gear, hospital fabrics, restaurants, and more settings where self-cleaning abilities are desirable. Further development could enable effective self-cleaning smart textiles enhanced with these multifunctional nanomaterials[9-13].

Chitosan is a cationic, naturally sourced biopolymer with known biocompatibility, biodegradability, nontoxicity, and inherent antimicrobial activity. As a coating agent, chitosan can bind strongly to negatively charged textile surfaces like cotton to impart durable functional properties. Furthermore, the addition of clay particles as well as metal oxide nanoparticles augments the multifunctional attributes achieved by chitosan coatings alone. Specifically, clay nanoparticles reinforce mechanical durability and flame retardant, ZnO nanoparticles exhibit strong broad-spectrum antimicrobial activity, and TiO2 nanoparticles offer self-cleaning ability through catalytic degradation as well as UV blocking functions [6, 14-24].

The aim of the present work was focused to investigate the added value incorporated when different Nanoparticles used to prepare multifunctional cotton fabric treated via two methods of chemical modification namely In Situ formation of CTS/NPs hybrid nanocomposite to Blank cotton fabrics & cationized cotton fabric which treated firstly with NaOH/quatt 188 in certain conditions. Coating processes for fabrics under investigation, such as dip coating, padding, layer-by-layer assembly, and ultrasonic irradiation, can impart textiles with nanoscale chitosan-clay ZnO-TiO2 films and coatings that are stable against washing and used conditions. Optimization of nanoparticle concentrations and uniform deposition lead to enhanced functionality. Recent investigation in this area aims to expand on these achievements to develop next-generation textiles with sustainable, versatile functions based on green, natural materials and scalable fabrication processes [6, 25-28].

2. Materials and Methods:

2.1. Materials

Plain weave mill-scoured and bleached 100% cotton fabric (220 g/m2) was used in this study. Nano-sized ZnO (ZnO-NPs, 50 wt.%, particle size < 35 nm avg.), nanosized TiO2 (TiO2, 0.02 mg/L, particle size 40 nm avg.), and clay nanoparticles were purchased from Sigma Aldrich. Commercial-grade water-soluble Chitosan (deacetylation 88%, M. Wt. 2.0 105, Acros Organics, NJ, USA) and Quat 188 (65%, cationic monomer, Dow Chem Co., Midland, Michigan, USA) were used as received. Laboratory-grade acetic acid and sodium hydroxide were used. Bi-distilled water was used for all preparations.

2.2. Preparation of chitosan coating layer

The experimental technique adopted for chitosan was as follows: Chitosan solution was obtained by dissolving (0-3) g in 100 mL of 1% wt citric acid/ sodium hypophosphite (CA)/SHP until complete dissolution.

2.3. Preparation of chitosan/ metal nanoparticles composite Cs/NPs:

The required amounts of Ti nanoparticles (0.5, 1.0, and 2.0%) were added to the chitosan dissolver on citric acid (2% W/V, initial concentration 20 g/l) during magnetic stirring. To prepare the nanocomposite, 2 ml of 2% Tween was added to the mixture, which was left under magnetic stirring for 1 hour. The solution was then poured into a sonicator for 2 hours to achieve good homogeneity and miscibility. The clay and zinc nanocomposites were prepared individually using the same method and concentrations.

2.3.1. Synthesis of CTS/NPs hybrid nanocomposite

CTS, NPs [under study individually], citric acid and sodium hypophosphite (SHP) were thoroughly mixed in water to form a slurry. Chitosan and NPs[under study individually] concentrations (w/v) ranged from [0.25-1% and 0.025- 0.1% respectively whereas citric acid was used at a concentration of 5% and SHP at 4%. The slurry was subjected to sonication. Sonication resulted in /CTS/NPs hybrid nanocomposite possibly through interaction layers of CTS. The ultimate nano-product was in the form of stable nano emulsion.

2.4. Fabric Treatment for Finishing
2.4.1. Pretreatment for cotton fabric
2.4.1.1. Scouring

To prepare the nanocomposite, 2 ml of 2% Tween was added to the mixture, which was left under magnetic stirring for 1 hour to allow proper mixing. The resulting solution was then sonicated for 2 hours to achieve good homogeneity and miscibility of the components. Clay and zinc nanocomposites were separately prepared following the same method and using the same concentrations.

2.4.2. Finishing cotton fabric with prepared nanocomposites (Cs/NPs) by sol-gel method 1st method:

Cotton fabric samples were immersed in various finishing formulations, namely a finishing bath containing CS/(Ti, Zn, and Clay Nanoparticles) in individually different concentrations for 15 min, padded to wet pick up 80%, dried at 100 °C for 5 min, and finally cured at 160 °C for 3 min.

2.4.3. In Situ formation of CTS/NPs hybrid nanocomposite

The synthesized hybrid nanocomposite (stable nanoemulsion) was applied to cotton fabric as per the pad-dry-cure

method. Thus the fabric was padded in the emulsion containing CTS/NPs ,Citric acid and SHP in two dips and two nips to a wet pickup 100% followed by drying at 80ºC for 5 min then cured at 15ºC for 3 min.

2.4.4. Finishing cotton fabric (Cs/NPs) /quatt188 Layer by Layer Method: 2nd method:

Cationization of the cotton fabric was carried out using pad-dry-cure method. Experimental procedure adopted was as follows, Quat-188 (3-chloro-2-hydroxyl propyl-trimethyl ammonium chloride was mixed in solution with sodium hydroxide. Cotton fabric was padded through this mix and squeezed to wet-pick up of 100%. The fabric was dried at 40ºC for 15 min and then cured at 120ºC for 15 min. At the end, the sample was washed with water several times and finally dried at ambient conditions. Fabric samples were padded twice in CTS/NPs hybrid nanocomposite as per the pad-dry-cure method

2.5. Testing and analysis
2.5.1. FT-IR spectra

Fourier transform infrared (FT-IR) spectra of the samples were obtained using a JASCO FT-IR-6100 spectrophotometer and the potassium bromide (KBr) pellet disk technique. The spectra were collected in transmittance mode in the 4000 to 400 cm^{-1} wavelength range at a resolution of 4 cm^{-1}.

2.5.2. Thermal analysis

Thermogravimetric analysis (TGA) was performed from 25°C to 600°C under inert nitrogen gas at a heating rate of 10°C/min using an SDT Q600 V20.9 Build 20 instrument (USA).

2.5.3. X-ray diffraction

X-ray diffraction (XRD) analysis of the samples was conducted using a STOE STADI P transmission X-ray diffractometer. The diffraction patterns were recorded over a 2θ angle range of 10° to 80° using monochromatic Cu Kα radiation with a wavelength of 1.54051 Å.

2.5.4. Mechanical and physical properties
2.5.4.1. Tensile strength

The tensile strength of the fabric samples was assessed following ASTM Test Method D5035 using a Q-Test 1/5 tensile tester. Three specimens were tested in the warp direction for each treated fabric. The average breaking load (Lb) recorded for the three specimens represented the tensile strength of each fabric. [29]

2.5.4.2. Breaking elongation

Breaking elongation is defined by Equation 2, where L0 is the initial length of the strip (strain gauge = 20 cm), L is the length of the strip at the breaking point, and E% is the breaking elongation. According to the standard testing conditions, the speed of the jaws was set to 50 mm/min.

$$E\% = [(L - L0) / L0] * 100 \qquad \text{Equation 2}$$

2.5.4.3. Air permeability

Breaking elongation is defined by Equation 2, where L0 is the initial length of the strip (with a strain gauge of 20 cm), L is the length of the strip at the breaking point, and E% is the breaking elongation percentage. According to the standard testing conditions, the speed of the jaws was set to 50 mm/min.

2.5.5. Scanning Electron Microscopy (SEM)

Scanning electron microscopy (SEM) and energy-dispersive X-ray spectroscopy (EDS) examinations of the fabric samples were performed using a Philips XL30 microscope equipped with a LaB6 electron gun and a Philips-EDAX/DX4 EDS system. SEM images were captured at various magnifications ranging from 150X to 3000X, depending on image clarity. To prepare samples for imaging, the fabrics were fixed on stubs with carbon glue and coated with a gold film using vapor deposition.

2.5.6. Transmission Electron Microscopy (TEM)

The morphology and dimensions of the nanoparticles were examined by transmission electron microscopy (TEM) using a JEOL-JEM-1200 instrument. TEM samples were prepared by depositing a drop of the colloidal nanoparticle solution onto 400 mesh copper grids coated with an amorphous carbon film. The solvent was allowed to

evaporate in air at room temperature. The average diameter of the nanoparticles was determined by measuring the diameter of 100 randomly selected nanoparticles in enlarged TEM micrographs.

2.5.7.   *Atomic absorption and UV-Protection*

The metal content (zinc, titanium, and silicon) of the coated fabric samples with ZnO NPs, TiO$_2$NPs, and SiO$_2$NPs was determined by a flame atomic spectrophotometer at GBC Avanta, Australia. The UV-protection factor (UPF) demonstrates the ratio of sunburn-causing UV measured without and with the protection of the fabric. The UPF of untreated and finished fabric samples (size 3 cm $\times$ 3 cm) was determined according to the Australian/New Zealand standard (AS/NZS 4399-1996: Sun protective clothing—Evaluation and classification) using a UV-Shimadzu 3101 PC spectrophotometer at a wavelength of 280–390 nm, which includes the UVB (280–320 nm) and the UVA (320–400 nm) according to the following equation: [30-35]

$$UPF_i = \frac{\sum\limits_{\lambda=280}^{400} E_\lambda \times S_\lambda \times \Delta\lambda}{\sum\limits_{\lambda=280}^{400} E_\lambda \times S_\lambda \times T_\lambda \times \Delta\lambda}$$

where: E λ = relative erythemal spectral effectiveness, S λ = solar spectral irradiance, T λ = average spectral transmission of the specimen, and $\Delta\lambda$ = measured wavelength interval (nm). Regarding UV protection categories, fabrics are classified as good, very good, or excellent if their UPF values range from 15 to 24, 25 to 39, and above 40 (40+), respectively.

2.5.8.   *Evaluation of Antibacterial activity*

2.5.8.1.   *Materials*

The microbial strains employed in this study included Escherichia coli (ATCC 25922) as a representative Gram-negative bacterium, Staphylococcus aureus (ATCC 6538) as a representative Gram-positive bacterium, and Candida albicans (ATCC 10231) as a pathogenic yeast. These strains were chosen for their frequent association with wound infections. Fresh inoculate for antimicrobial testing were prepared by cultivating each strain in nutrient broth at 37°C for 24 hours.

2.5.8.2.   *Test methods*

To ensure reproducibility, all antibacterial activity tests were performed in triplicate. The finished fabrics' antibacterial activity against S. aureus and E. coli was determined using the colony counting method.[36] where 0.5 g of peptone and 0.3 g of beef extract were combined with 100 ml of water to create a liquid culture. Samples of blended films

with a diameter of 1 cm were cut, and 10 milliliters of liquid culture were added, along with 10 microliters of microbe culture. Every sample was incubated at 37 °C for 24 hours. A 100-µl solution was extracted from each incubated sample, diluted, and then spread out onto an agar plate. All plates were incubated for 24 hours, and the colonies formed were counted. Following is the calculation of the percentage bacterial reduction: [32, 37-50]

$$\text{Reduction in CFU (colony forming units)\%} = \frac{C - A}{C} \times 100$$

In this case, C is CFU/ml at zero contact time and A is CFU/ml after contact (end test).

2.5.9.   *Self-cleaning action of TiO$_2$NPs loaded fabrics.*

The self-cleaning ability of the TiO2NPs was tested by exposing fabric samples stained with methylene blue (MB) dye to sunlight. One half of each stained fabric sample was irradiated with sunlight for 48 hours, while the other half was covered with black paper to prevent sunlight exposure. The sunlight-exposed stained region was compared to the covered stained region to evaluate the self-cleaning action. The colour strength, expressed as K/S values, of untreated and TiO2NP-loaded fabric samples was measured before and after sunlight exposure. K/S values are directly proportional to the amount of dye present on the fabric. A decrease in K/S values indicates degradation of the dye stains due to the self-cleaning effect of the TiO2NPs under sunlight irradiation[51], according to equation (1): [42, 46, 52-56]

$$\text{Extent of discoloration(\%)} = \frac{(K/S)a}{(K/S)b} \times 100 \quad (1)$$

where (K/S)b represents colour strength prior to daylight exposure and (K/S)a represents colour strength following daylight exposure.

3.   Results and Discussion:

3.1.   Preparation equation of coating prepared 1st & 2nd Methods
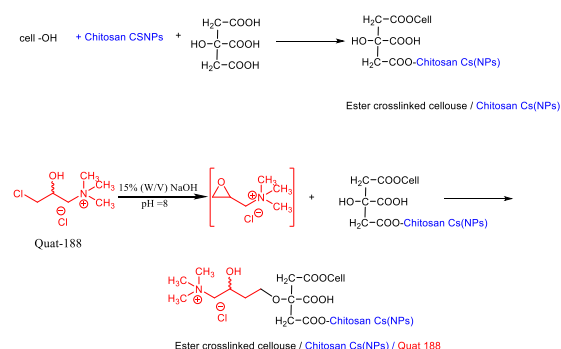
3.2. FTIR

The chemical composition of cotton fabrics, encompassing the nature of linking bonds, the presence of specific functional groups, and its segment structure, significantly influences its physicochemical properties and performance in intended applications. Fourier Transform Infrared (FT-IR) spectroscopy was employed to deepen our understanding of the effects of chemical finishing on the cotton fabric's chemical structure (Figures 1-3).

Figure 1 displays the FTIR spectra of cotton fabrics, with easily identifiable peaks corresponding to cellulose, lignin, and hemicellulose. The strong, broad peak at 3330 cm-1 is attributed to water, lignin, and cellulose hydroxyl (OH) groups. The C-H stretching vibrations in cellulose and hemicellulose contribute to the peak at 2893 cm^{-1}. The presence of water in the fibers is indicated by the band at 1643 cm^{-1}. The absence of a peak at 1730 cm^{-1}, associated with hemicellulose's carboxyl groups, aligns with TGA data indicating low hemicellulose content in cotton.

The peak at 1427 cm^{-1} is attributed to cellulose's CH_2 symmetric bending. The aromatic rings of cellulose polysaccharides exhibit C-H and C-O bending vibrations, manifesting as bands at 1363 and 1333 cm^{-1}. The sharp peaks in the spectra provide valuable insights into the intricate chemical structure of cotton fabrics under different chemical finishing treatments. [57-61].
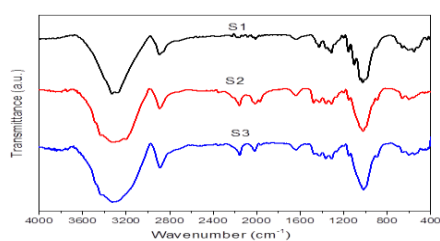
Figure 1 :FTIR spectrum of cotton blank (S1), cotton fabrics treated with chitosan (Cs /NPs) (S2) cotton fabrics treated with (Cs /NPs /quatt) (S3)

The FTIR spectrum of cotton fabric (Figure 1 S2) showed characteristic peaks indicating peaks at 3400 cm^{-1}, indicating the presence of a free carboxylic group of citric acid; additional peaks related to O-H (3329, 3281 cm^{-1}); C-H (2159 cm^{-1}); and C=O amine stretches (1643 cm^{-1}), verifying persistent physical and chemical alteration of the cellulose by chitosan. The FTIR spectrum of cationized cotton treated first by chitosan treatment [2nd method] is shown in figure 1 S3 and displays the key peaks, which include C-H stretch (2891 cm^{-1}), C-N stretch (1210 cm^{-1}), and $N^+(CH_3)_3$ stretches (1746–1536 cm^{-1}), confirming the fixation of quatt188. [62, 63]
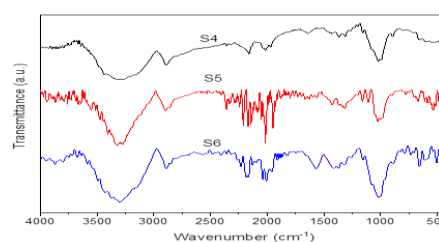
Figure 2 :FTIR spectrum of the cotton fabric treated with chitosan and finished with titanium nanoparticles (S4), clay nanoparticles (S5) and zinc oxide nanoparticles (S6) in 1st method

Figure 2 depicts the FT-IR spectra of cotton fabrics treated with titanium nanoparticles (S4), clay nanoparticles (S5), and zinc oxide nanoparticles (S6) through dry cure fixation pretreatment in 1st method. Common characteristic peaks such as O-H stretches at 3273 cm^{-1}, C-H stretches at 2932 cm^{-1}, and non-hydrated C=O stretches at 1700 cm^{-1}, indicative of cellulose presence, were observed in all fabric samples. The TiO_2 nanoparticles treated fabric exhibited red-shifted peaks, suggesting hydrogen bond deformation and Ti-O bond formation, with a shifted O-H vibration band at higher wavenumbers, indicating cellulose-TiO_2 nanoparticle bonding. This affirms the adsorption of TiO_2 nanoparticles onto the cellulose fabric, enhancing its qualities. Comparing clay nanoparticle-treated and TiO_2 nanoparticle-treated fabrics, similar transmittance (95%) was observed, but new bands in the C=O absorption band range were noted in the former, with a transmittance of 90%, indicating photo-catalytic improvement in TiO_2 nanoparticle-treated fabric. In "S4," absorption bands at 1082 cm^{-1} and 709 cm^{-1} indicate the presence of Ti–O–Si and Ti–O–Ti, revealing the hydrolyzed GPTMS on the fabric surface bonded with amino groups during curing. "S6" illustrates the FTIR spectra of ZnO nanoparticle-treated fabrics, with peaks at 1420 and 900 cm^{-1} attributed to cellulose bending and a Zn–O stretching frequency at 451 cm^{-1}, confirming nano-ZnO formation on cationized cotton fabric[64-71].
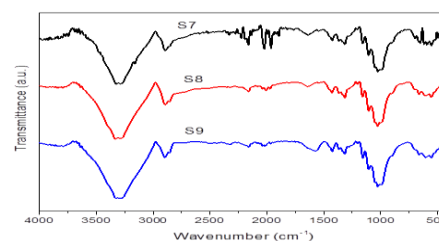
Figure 3 :FTIR spectrum of the cotton fabric treated with chitosan (Cs/NPs/quatt) as titanium nanoparticles (S7), clay nanoparticles (S8) and zinc oxide nanoparticles (S9) in 2nd method

Fig. 3 represents the FT-IR spectra of the cationized modified cotton fabrics treated with titanium nanoparticles, (S7), clay nanoparticles (S8), and zinc oxide nanoparticles (S9) via dry cure fixation pretreatment in the second method, as mentioned in the experimental part. FT-IR spectra show that cotton fabrics treated with titanium oxide nanoparticles, clay, and zinc oxide nanoparticles in the presence of quat-188 and chitosan in the 2nd method have characteristic band peaks similar to those prepared in the 1st method, with differences in their band peak intensities.

3.3. Thermal Analysis

The results obtained from thermogravimetric analysis (TGA) of the modified cotton fabrics treated in 1st method are shown in Figure 4 [72, 73]. The TGA thermograms of all samples were identical to those of cotton fibres and showed two main weight loss regions. The evaporation of water and some substances that are physically bonded to the fibres is responsible for the initial weight loss that is seen between 30 and 110 °C. The breakdown of the fiber's cellulose is connected to the second weight loss phase, which is linked to the maximal decomposition rate at 360 °C. An extra weight loss process is sometimes observed in some natural fibres in the 220-310 °C range related to the presence of hemicellulose. The composition of cotton is ~90% cellulose, ~6% hemicellulose, and 4% extractives, lignin, and waxes.. The first stage is due to the evaporation of adsorbed moisture, which occurs between 35– 157 °C; 36-161 °C, 36-151 °C, and 34-137 °C at the peak's maxima at 89 °C, 97 °C, 95 °C, and 75 °C, which corresponds to 2.2745 %, 3.294 %, 3.165%, % and 2.096% weight loss for blanks, titanium nanoparticle-treated cotton fabrics, clay treated cotton fabrics, and zinc oxide treated cotton fabrics in the first method. This is evident from the downward slope of the TGA curve during this temperature range.
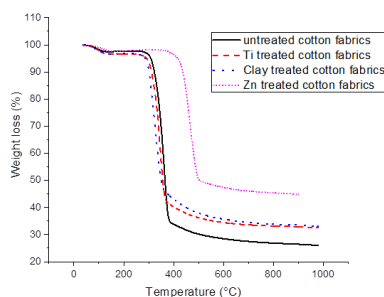
Figure 4 : Thermogravimetric analysis TGA thermogram expressed in weight loss of untreated &treated cotton fabrics with titanium nanoparticles, clay nanoparticles and zinc oxide nanoparticles in 1st method

The thermal behaviour diagram of cotton fabrics before and after treatment with titanium, clay, and zinc oxide in the second method is shown in Figure 5. The TG curves demonstrated that untreated and treated cotton fabrics show two main weight loss stages. The first stage is due to the evaporation of adsorbed moisture, which occurs between 35–157 °C, 37–146 °C, 36–146 °C, and 36–133 °C at the peak's maxima at 89 °C, 76 °C, 91 °C, and 74 °C, which corresponds to 2.2745%, 0.041%, 1.845%, and 0.89% weight loss for blanks, titanium nanoparticles treated cationized cotton fabrics, clay treated cationized cotton fabrics, and zinc oxide treated cationized cotton fabrics in the 12th method. This is evident from the downward slope of the TGA curves during this temperature range.
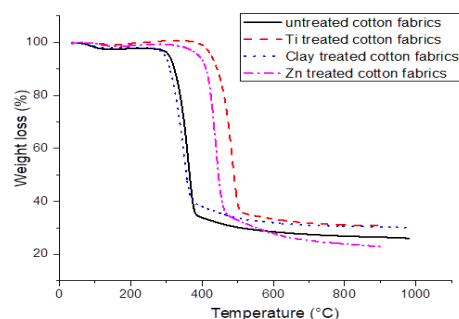
Figure 5 : Thermogravimetric analysis TGA thermogram expressed in weight loss of untreated /cationized cotton fabrics, titanium nanoparticles, clay nanoparticles and zinc oxide nanoparticles in 2nd method

3.4. XRD analysis

The powdered TiO2 NPs XRD pattern is shown in Figure 6. In the anatase TiO2 phase, anatase peaks can be seen at 2θ values of 52.47°, 55.05°, 63.44°, 74.50°, and 76.50°, corresponding to the crystal faces (105), (211), (204), (215), and (301), respectively (JCPDS card #21-1272). Rutile peaks, corresponding to the crystal planes (001), (110), (210), and (221), are seen at 2θ values of 14.42°, 29.62°, 44.48°, and 66.75° (JCPDS card #21-1276). Interestingly, the anatase phase is maintained at 150°C, however beyond 250°C, the rutile phase becomes predominant.[74, 75]. Figure 6. Also shows the appearance of TiO_2 peaks in treated cotton fabrics via step by 1st and 2nd method which confirm the presence of nanoparticles on the surface as well as in the fabrics bulk. Overall, the results of XRD patterns indicated that anataseTiO$_2$ nanoparticles were successfully loaded on the cotton fabrics in both methods studied.
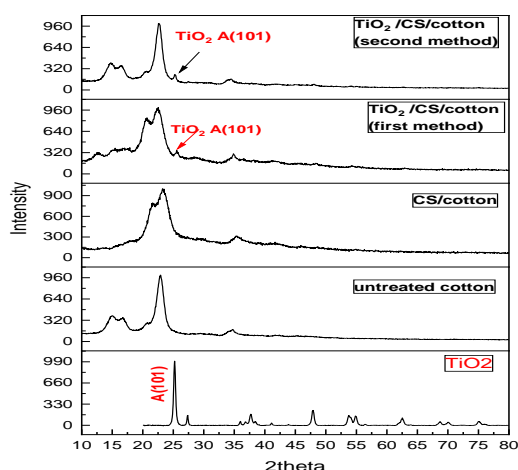
Figure 6: XRD pattern of TiO_2 nanoparticles, untreated cotton fabrics, chitosan treated cotton fabrics, TiO_2/chitosan treated cotton fabrics in 1st &2nd Method

The XRD patterns of the ZnO nanocrystalline powder are displayed in Figure 7. The sharp, intense peaks of ZnO resulting from the hexagonal ZnO reflections - (100), (002), (101), (102), (110), (103), (200), (112), and (201) - confirm the good crystalline nature of the material.[76]. Additionally, Figure 7 does not show the crystal structure of ZnO nanoparticles in cotton fabrics treated with chitosan and ZnO under either method. This suggests that the ZnO nanoparticles are present inside the treated cotton fabrics rather than on the surface. [77]. Overall, the XRD results indicated that ZnO nanoparticles were successfully loaded inside the cotton fabrics, not on the surface, for both methods studied.
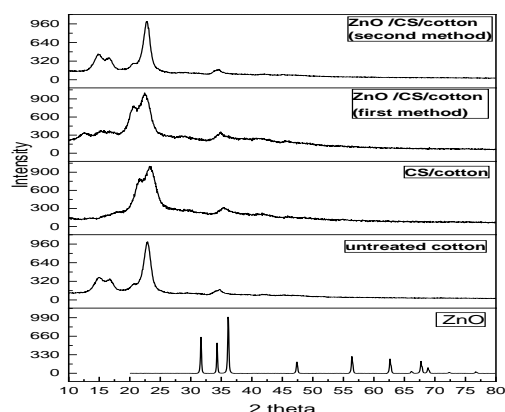
Figure 7: XRD pattern of ZnO nanoparticles, untreated cotton fabrics, chitosan treated cotton fabrics, ZnO/chitosan treated cotton fabrics in 1st&2nd method

X-ray diffraction (XRD) measurement results of the clay nanoparticles are shown in Figure 8. Diffraction peaks are observed for the clay corresponding to basal spacings of d001524.17 Å (2θ=53.88°) and d002511.90 Å (2θ=57.32°) (Figure 8). The results are comparable to those reported by Golebiewski et al.[77]. Whereas the XRD pattern of cotton fabrics treated with chitosan and clay shows the presence of a clay crystal pattern in the treated fabrics in the 1st method and is not found in the XRD pattern of the 2nd method, this is due to the fact that cotton fabrics have a higher affinity for chitosan than clay. Overall, the results of the XRD patterns indicated that clay nanoparticles were successfully loaded on the cotton fabrics in the first method of treatment and inside the cotton fabrics in the second method.
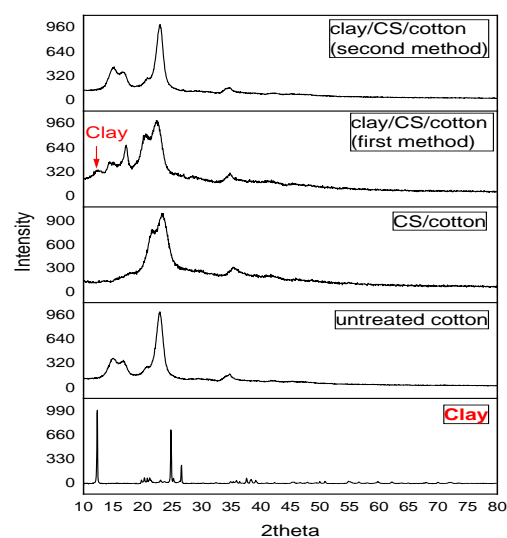
Figure 8: XRD pattern of clay nanoparticles, untreated cotton fabrics, chitosan treated cotton fabrics, clay/chitosan treated cotton fabrics in 1st &2nd method

3.5. Mechanical and physical properties
3.5.1. tensile strength

The graph depicts the effect of titanium nanoparticle finishing on the tensile strength of fabrics. Initially, the tensile strength increased after coating fabrics with quatt, with samples showing a force of 95 kF. However, the tensile strength began to decrease after the TiO_2 NPs were finished. It is clear that the increased concentration of TiO_2 molecules leads to a further decrease in the overall tensile strength of both methods. In the second method, the C1 sample showed the highest value, while the C2 and C3 samples showed the lowest value. A significant reduction in tensile strength was observed, where the tensile strength decreased to 65 kF in the C1 sample. As the TiO_2 concentration

increased, the tensile strength decreased to 55 kF in the C2 and C3 samples, with no significant difference between the two samples. In the second method, the C1 and C2 samples showed the highest value, while the C3 sample showed the lowest value. The C1 and C2 samples showed a value of 40 kF, and the C3 sample showed 39 kF. Notably, there was no significant difference in the tensile strength of the samples treated in the second way. However, the samples treated in the second method showed much lower tensile strength values than the samples treated in the first method (Figure 9).
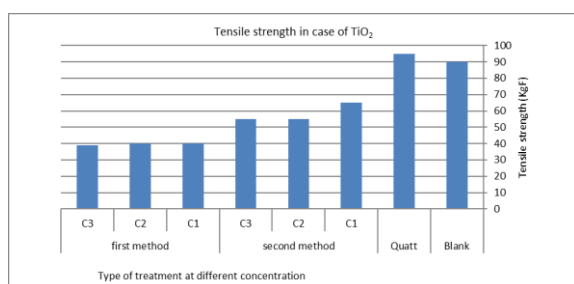
Figure 9: Tensile strength of blank cotton, cationized cotton,(C1,C2,C3) treated cotton with different conc TiO_2 NPs (1st & 2nd method) respectively.

Figure 10 displays the effect of finishing fabrics with clay NPs on their tensile strength. Overall, the tensile strength decreased after the clay nanoparticle treatment. The extent of this decrease varied depending on the concentration and the treatment method followed. The first method, which involved a gradual increase in the concentration of nanoparticles, resulted in a decrease in the tensile strength. The values attained were 85 KgF, 80 KgF, and 60 KgF for samples C1, C2, and C3, respectively. It was observed that the highest value was attained for sample C1, while the lowest value was attained for sample C3, which represented the highest concentration. However, this decrease was not significant compared to the second method, which involved one path. In this method, the tensile strength decreased significantly with an increase in concentration. The values attained were 50 KgF, 34 KgF, and 27 KgF for samples C1, C2, and C3, respectively. It is worth noting that while sample C1 had the highest value, this value decreased in sample C2, and this decrease continued in sample C3. The tensile strength of the first method decreased by almost 36% in the high concentration, while the second method's decrease was about 70%. This shows the difference between the two methods in influencing the tensile strength of the fabrics (Figure 10)
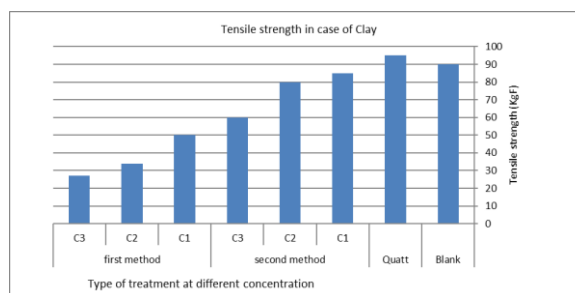
Figure 10: Tensile strength of blank cotton, cationized cotton, (C1,C2,C3) treated cotton with different conc clay NPs (1st & 2nd method) respectively

Figure 11 above illustrates the impact of zinc nanoparticle finishing on the tensile strength of the fabric. Generally, the tensile strength of the fabric decreased after treatment with ZnO NPs. In the second method, the tensile strength gradually decreased as the concentration of nanoparticles in the fabric increased. The tensile strength decreased slightly to 90 KgF in the C1 sample, then to 88 KgF in the C2 sample, and finally to 85 KgF in the C3 sample. However, the tensile strength of the fabric was not significantly affected, as the value in the untreated sample was 90 KgF, which was only 5.6% in the high concentration. The first method showed a greater reduction in tensile strength. This reduction increased gradually as the concentration of ZnO molecules in the fabric increased. The values of tensile strength in the C1, C2, and C3 samples were 64 kF 63KgF and 55KgF, respectively. Here, C1 represents the highest value, and C3 represents the lowest value. It can be stated that in the first method, the tensile strength decreased by approximately 38.8% in the high concentration. (Figure 11).
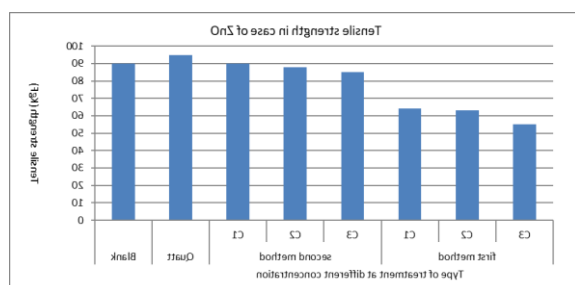
Figure 11: Tensile strength of blank cotton, modified cotton, (C1,C2,C3) treated cotton with different conc ZnO NPs (1st & 2nd method) respectively.

3.5.2. *Elongation at break*

Figure 12 demonstrates the impact of treatment with titanium nanoparticles on the breaking elongation of fabrics. As shown in the figure, there

_____

Egypt. J. Chem. **67,** SI: M. R. Mahran (2024)

are significant differences in the breaking elongation of fabrics between nano-finished and unfinished specimens. Generally, elongation decreases after titanium nanotreatment. Initially, there was a significant increase in elongation in the Quatt sample (35%), compared to the Planck sample (20%). For the second treatment method, the C1 sample had the highest value (35%), the C3 sample had the lowest value (15%), and the C2 sample had a value of 20%. It is noticeable that the elongation gradually decreases as the concentration of titanium nanoparticles in the samples increases. However, the elongation was not much less than that of the blank fabric, even with a high concentration of nanoparticles. For the first treatment method, the C1 sample had the highest value (15%), while the C3 sample had the lowest value (10%).

Here also, it is noticeable that the elongation decreases as the concentration of nanoparticles in the samples increases, but the elongation values here are much lower than in the second method. (figure 12).
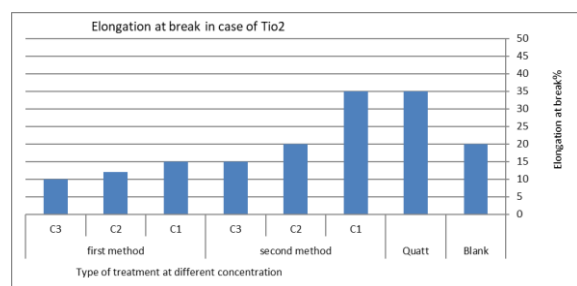
Figure 12: Elongation at break of blank cotton, modified cotton, (C1, C2,C3) treated cotton with different conc Tio2 NPs (1ˢᵗ &2ⁿᵈ method) respectively.

Figer 13Figure 14 above illustrates the impact of zinc nanoparticle finishing on the elongation of fabrics. Generally, the elongation improved after nanofinishing, especially with lower concentrations. In the second method, the C1 sample had the highest value of elongation (40%), followed by the C2 sample (38%), and the C3 sample had the lowest value (28%). In comparison with the blank sample, the elongation generally increased in the second method, even after decreasing with high concentration. On the other hand, in the first method, the elongation was not significantly affected, with the C1 sample showing the highest value of elongation (23%), and the C2 and C3 samples having the same value (20%), which is the same as the elongation value in the blank sample. Compared to the two methods, the second method could be said to have improved the fabric's elongation even as the concentration increased, while the first method did not decrease much and did not underestimate the elongation value of the untreated fabric. (figure14.)

presented above displays the impact of clay nanoparticle treatment on the breaking elongation of fabrics. Method two resulted in an overall improvement in elongation after the treatment with clay nanoparticles, especially at lower concentrations. The C1 sample showed the highest value of 40%, while the C2 sample showed a value of 38%. The C3 sample, however, showed a decrease in elongation to 15%. On the other hand, method one resulted in a decrease in elongation in general. The C1 sample exhibited the highest value of 20%, with no decrease in elongation at the lowest concentration. The C2 sample showed a value of 12%, while the C3 sample had the lowest value of 10%. It is noteworthy that at lower concentrations, there was a particularly noticeable difference between the effects of the first and second methods (Figure13).
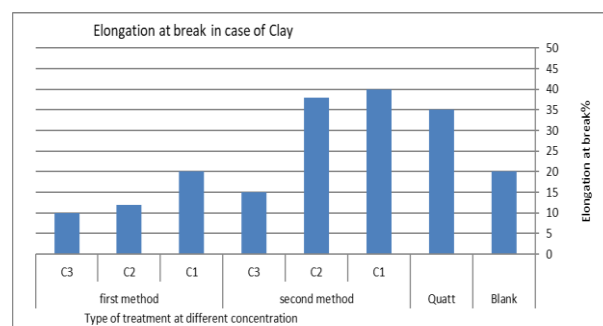
Figure 13.: Elongation at break of blank cotton, modified cotton,(C1,C2,C3) treated cotton with different conc clay NPs (1ˢᵗ &2ⁿᵈ method) respectively.

Figure 14. above illustrates the impact of zinc nanoparticle finishing on the elongation of fabrics. Generally, the elongation improved after nano finishing, especially with lower concentrations. In the second method the C1 sample had the highest value of elongation (40%), followed by the C2 sample (38%), and the C3 sample had the lowest value (28%). In comparison with the blank sample, the elongation generally increased in the second method, even after decreasing with high concentration. On the other hand, in the first method), the elongation was not significantly affected, with the C1 sample showing the highest value of elongation (23%) and the C2 and C3 samples having the same value (20%), which is the same as the elongation value in the blank sample. Compared to the two methods, the second method could be said to have improved the fabric's elongation even as the concentration increased, while the first method did not decrease much and did not underestimate the elongation value of the untreated fabric. (figure14.)

Figure 14: Elongation at break of blank cotton, modified cotton, (C1,C2,C3) treated cotton with different conc ZnO NPs (1st &2nd method) respectively

3.5.3. *Air permeability*

The graph depicts the impact of treating fabric with titanium nanoparticles on the air permeability of the fabric. The graph displays that the fabric has a high air permeability after the finishing process. It is also noticeable that as the concentration of TiO_2 increases in both methods, the air permeability of the fabric also increases. Initially, the air permeability of the fabric increased after processing it with quatt, and the value increased from 102 cm^3/cm^2 S to 166 cm^3/cm^2 S. In the first method, the C1 sample shows the lowest value, while the C3 sample shows the highest value. It is worth noting that by increasing the concentration of TiO_2 NPs, the air permeability of the fabric increased in the C1, C2, and C3 samples, where the values were approximately 191, 212, and 238 cm^3/cm^2 S , respectively. In the second method, it was observed that the C1 sample had a lower air permeability of 184 cm^3/cm^2 S while the C3 sample had a higher permeability of 215 cm^3/cm^2 S. The C2 sample had an air permeability of 196 cm^3/cm^2 S . This indicates that air permeability increased with the concentration of TiO_2 NPs. It is worth noting that the air permeability values in the first method were significantly higher than in the second method. This leads us to conclude that the first method significantly increased the air permeability of the fabric in the second method, with an increase of about 30%. On the other hand, the second method increased the air permeability by about 22% (Figure 15).

The graph displays how the air permeability of the fabric is affected by the treatment with clay nanoparticles. Generally, the air permeability of the fabric increased after the treatments. Specifically, it was observed that air permeability increased significantly after the treatment of the fabric with quatt from 102 to 166 cm^3/cm^2.S. The shape of the graph also shows the increase in air permeability after the treatment of the fabric with clay nanoparticles in both methods. In the first method (step by step), air permeability in the samples C1, C2, and C3 increased as the concentration of clay NPs

increased. The C1 sample had the lowest air permeability of 215 cm^3/cm^2 S , while the C2 sample had 227 cm^3/cm^2 S . The C3 sample had the highest air permeability value of 298 cm3/cm2.s, which was significantly higher than the values of C1 and C2. In the second method (one path), there was also an increase in air permeability as the concentration of clay NPs increased. The air permeability values in samples C1, C2, and C3 were 176, 194, and 236 cm^3/cm^2 S respectively. In the C1 and C2 samples, the difference between them was not significant, while the value in the C3 sample increased significantly. As seen from the graph, the increase in air permeability in the first method was much higher than in the second method, increasing by approximately 65.7% in the first method, while in the second method it increased by about 56.7% (Figure 16.)
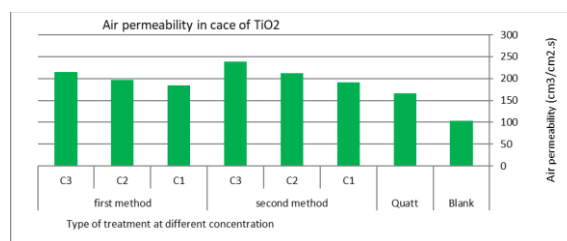
Figure 15: Air permeability of blank cotton, cationized cotton,(C1,C2,C3) treated cotton with different conc Tio2 NPs (1st &2nd method) respectively
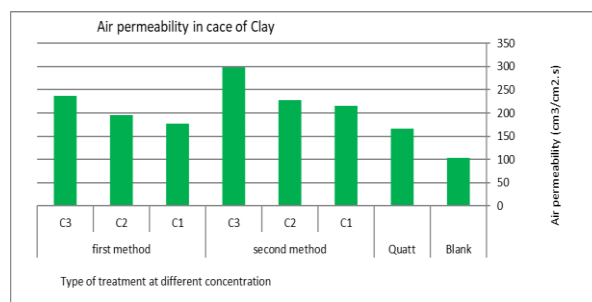
Figure 16: Air permeability of blank cotton, cationized cotton, (C1, C2, C3) treated cotton with different conc clay NPs (1st & 2nd method) respectively.

Figure 17. depicts the impact of zinc nanoparticles finishing on the air permeability of fabrics. It shows that increasing the concentration of Zn NPs in treatments leads to an increase in air permeability. In the first method (step by step), air permeability values increased significantly with an increase in the concentration of Zn NPs. The C1, C2, and C3 samples had permeability values of 211, 241, and 304 cm^3/cm^2 S , respectively. The highest air permeability value was seen in the C3 sample while

the lowest value was seen in the C1 sample. Furthermore, the air permeability increased significantly in higher concentration compared to lower concentrations in the C1 and C2 samples. In the second method (one path), the values for the C1, C2, and C3 samples were between 197, 201, and 245 cm^3/cm^2 S , respectively. The C3 sample had the highest value while there was no significant difference in the air permeability values of the C1 and C2 samples. It is worth noting that the increase in air permeability in the second method was less than in the first method, especially in higher concentrations. After the first treatment, air permeability increased by 66.4%, while after the second treatment, it increased by 58.3% in high concentration (Figure 17.)
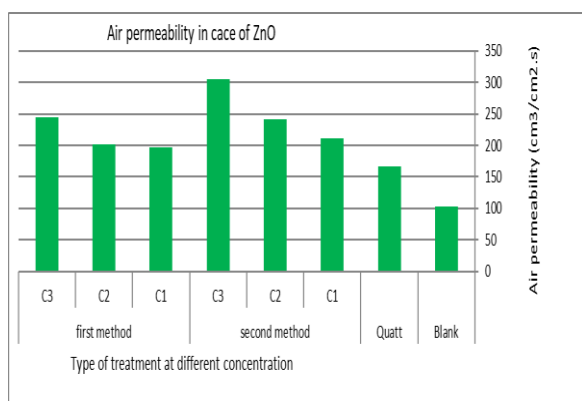
Figure 17. Air permeability of blank cotton, cationized cotton, (C1, C2, C3) treated cotton with different conc ZnO NPs (1st &2nd method) respectively

3.6. SEM & EDX analysis

The alterations in the surface morphology and elemental composition of untreated cationized cotton fabrics (Figures 18) are depicted, along with their treatment with TiO$_2$ nanoparticles (Figures 19 and 22), MMT clay nanoparticles (Figures 20 and 23), and ZnO nanoparticles (Figures 21 and 24). The SEM images illustrate the presence of ribbon-shaped cotton fibres and surface deposits resulting from the treatment of CS/NPs quatt-188 on the cotton fabrics. There is a noticeable change in surface morphology, with increased surface deposits directly attributed to the introduction of nanoparticles into the cotton fabrics (Figure 20). Additionally, a uniform, homogenous, and smooth surface coating is evident, indicating the positive coating ability of the post-loaded nanoparticles.
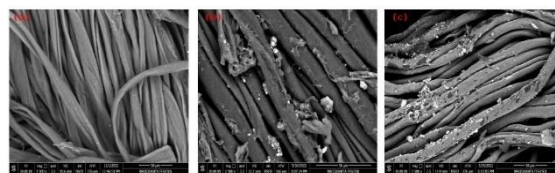
Figure 18: SEM images of (a)cotton blank, (b) cotton treated 1st method, (c)cotton treated 2nd method
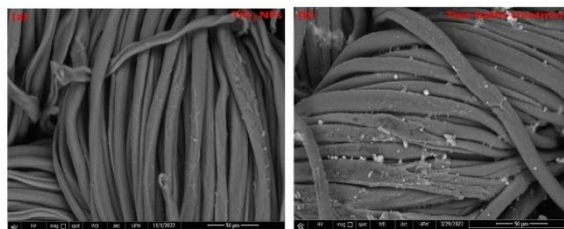
Figure19: SEM images of 1 wt. % TiO$_2$ nanoparticles treated cationized cotton fabrics (a) and 2 wt. % TiO$_2$ nanoparticles treated cationized cotton fabrics (b) in 2nd Method treatment.
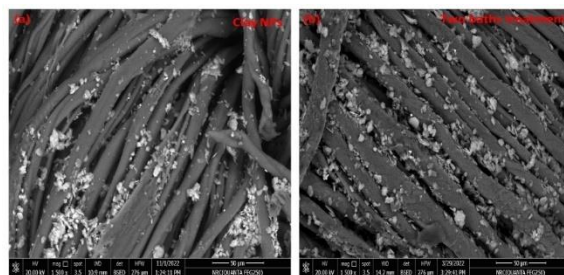
Figure 20: SEM images of 1 wt. % clay nanoparticles treated cationized cotton fabrics (a) and 2 wt. % clay nanoparticles treated cationized cotton fabrics (b) in 2nd Method treatment.
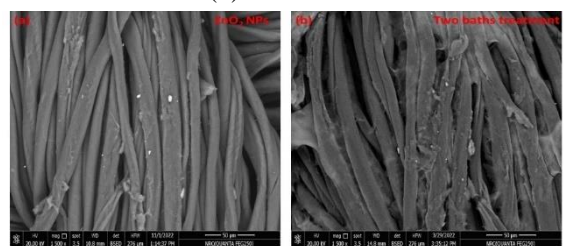
Figure 21: SEM images of 1 wt. % ZnO nanoparticles treated cationized cotton fabrics (a) and 2 wt. % ZnO nanoparticles treated cationized cotton fabrics (b) in 2nd Method .
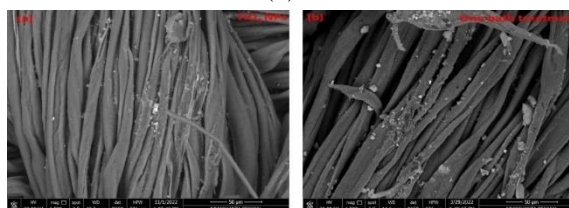
Figure 22: SEM images of 1 wt. % TiO$_2$ nanoparticles treated cationized cotton fabrics (a) and 2 wt. % TiO$_2$ nanoparticles treated cationized cotton fabrics (b) in 1st Method treatment.
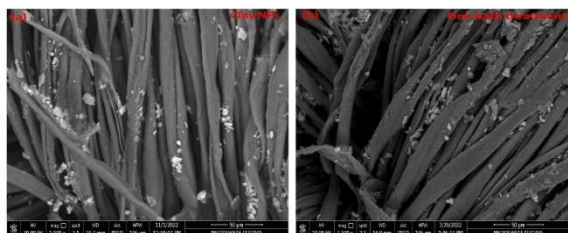
Figure 23: SEM images of 1 wt. % clay nanoparticles treated cationized cotton fabrics (a) and 2 wt. % clay nanoparticles treated cationized cotton fabrics (b) in 1st Method
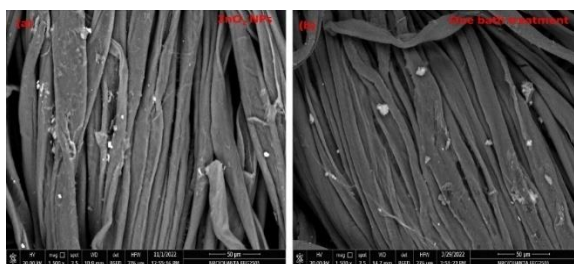
Figure 24: SEM images of 1 wt. % ZnO nanoparticles treated cationized cotton fabrics (a) and 2 wt. % ZnO nanoparticles treated cationized cotton fabrics (b) in 1st method

Additionally, EDX spectra of treated cotton fabrics with chitosan/NPs (Figure 25) confirm the treatment of chitosan/NPs onto cotton fabrics during the pre-modification step, expressed as N-element. Figures (26-28) confirm the existence of Ti, Si, and Zn elements as a direct consequence of the treatment of these nanoparticles into cotton fabrics in the first method, as well as the presence of these elements, which again confirm the successful loading of nanoparticles into cotton fabric surfaces in the second method, as shown in Figures (29-31).
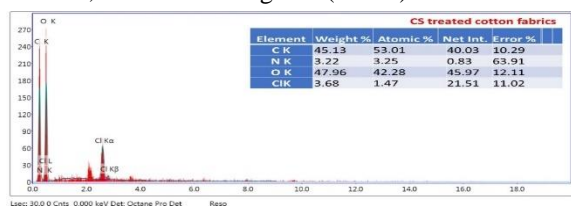
Figure 25. EDX spectra of treated cotton fabrics with quat-188/chitosan (cationized cotton fabrics)
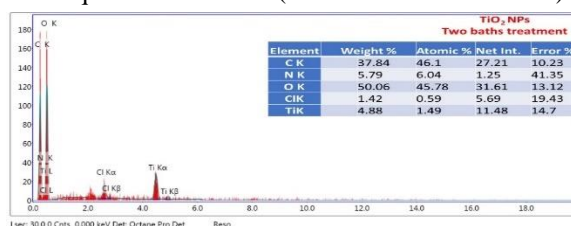
Figure 26. EDX spectra of 2 wt. % TiO$_2$ nanoparticles treated treated cotton fabrics in 1st method treatment.
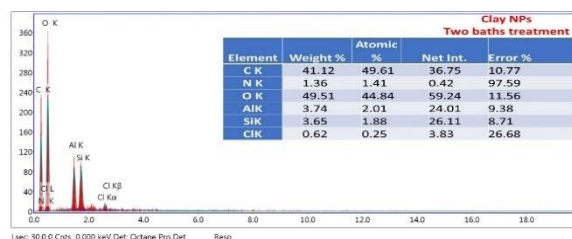
Figure 27. EDX spectra of 2 wt. % clay nanoparticles treated cationized cotton fabrics in 1st method treatment.
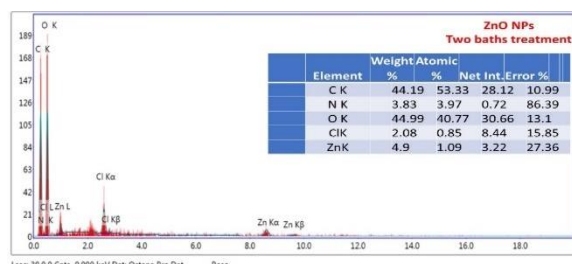
Figure 28. EDX spectra of 2 wt. % ZnO nanoparticles treated cationized cotton fabrics in 1st method treatment.
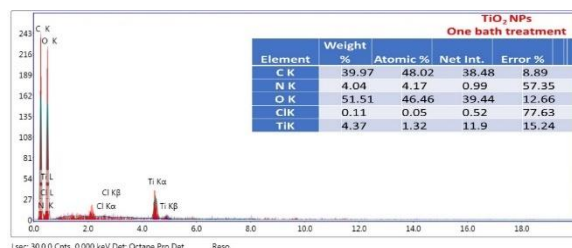
Figure 29. EDX spectra of 2 wt. % TiO$_2$ nanoparticles treated cationized cotton fabrics in 2nd method treatment.
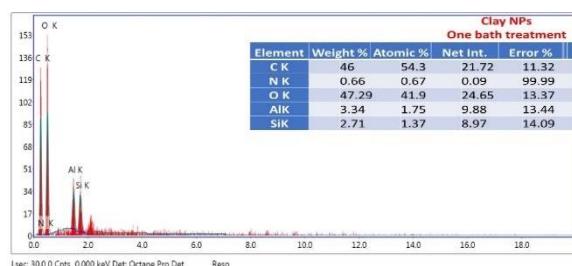
Figure 30. EDX spectra of 2 wt. % clay nanoparticles treated cationized cotton fabrics in 2nd method treatment.
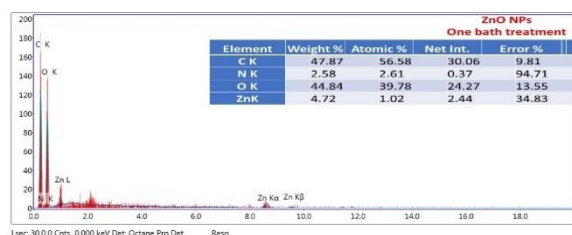
Figure 31. EDX spectra of 2 wt. % ZnO nanoparticles treated cationized cotton fabrics in 2nd method treatment.

Also, EDX spectra confirms the high deposition of elements on cationized cotton fabrics in first treatments than that for second treatment for both (TiO_2 nanoparticles, clay nanoparticles and ZnO nanoparticles).

3.7. TEM imaging analysis

TEM analysis of ZnO nanoparticles treated cotton fabrics has been made in Figure 32. ZnO nanoparticles were discovered to be embedded in cotton bristles, and a selective electron diffraction (SAED) pattern demonstrated the development of the Wurtzite structure of ZnO [71]. In addition, a new coating layer based on ZnO nanoparticles loaded chitosan were developed to obtain a powerful antibacterial system to prevent their side effects.
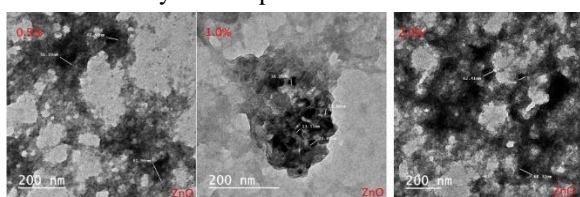
Figure 32: Transmission electron micrograph (TEM) of cotton fabrics embedded with ZnO nanoparticles at three different concentrations 0.5 wt.%, 1.0 wt.% and 2.0 wt.%

The Wurzite structure development of ZnO is revealed by the selected area electron diffraction (SAED) pattern in Figure 1. and the particle size ranged from 30-42 nm for a concentration of 0.5 wt. %, 22–35 nm for a concentration of 1.0 wt. %, and 49–89 nm for a concentration of 2.0 wt. %. Therefore, the nanoparticles at concentrations of 1.0 wt. % have the lowest particle size distribution. Additionally, a potent antibacterial system was created by covering clay nanoparticles and TiO2 nanoparticles loaded with chitosan, as demonstrated in Figures 2 and 3 for the former and the latter, respectively. This helped to avoid any negative side effects. Figure 33 shows the morphology of clay nanoparticles with particle sizes ranging from 19.5–54.5 nm at a concentration of 0.5 wt.% clay nanoparticles, from 30-142 nm at a concentration of 1.5 wt.% clay nanoparticles, and from 24–49.5 nm at a concentration of 2.0 wt.% clay nanoparticles.
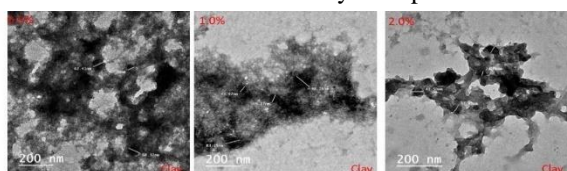
Figure 33: Transmission electron micrograph (TEM) of cotton fabrics embedded with clay nanoparticles at three different concentrations 0.5 wt.%, 1.0 wt.% and 2.0 wt.%

The shape of TiO_2 nanoparticles is depicted in Figure 34. The morphology of TiO_2 nanoparticles is remarkably homogeneous, with a mostly spherical and uniform particle size distribution (Figure 34). The particle size is ranging from 32-45 nm at concentration 0.5 wt.%, 17-22 nm at concentration 1.0 wt.% and 14-19.5 nm at concentration 2.0 wt.%. Therefore, TiO_2 nanoparticles with concentration 2.0 wt.% has the best particle size distribution.
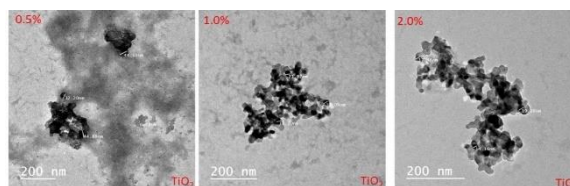
Figure 34. Transmission electron micrograph (TEM) of cotton fabrics embedded with TiO_2 nanoparticles at three different concentrations 0.5 wt.%, 1.0 wt.% and 2.0 wt.%

3.8. Atomic absorption and UV-Protection

For a given two main sets of finishing in two methods, the data in Table 1 demonstrate the inclusion of nanofinishing with different metal nanoparticles, such as Ti as TiO_2 nanoparticles, Si as SiO_2 nanoparticles, and Zn as ZnO nanoparticles. The results show an increase in the metal content as the concentration of metal nanoparticles increases in two ways. The amount of metal deposited in cotton fabrics in the first treatment is greater than that for the second treatment in one bath, which reflects the fabric inherent towards finishing materials. In addition, the increase in metal content within the fabric surface agrees with the data of EDS and proves the self-cleaning, ultraviolet protection, and antibacterial properties of the treated cotton fabrics. [9, 78]. The ultraviolet protection value of untreated cotton fabric is 3.53, and their values increased as metal content increased, as shown in Table 1, in the same manner. Table 1 illustrates that the UPF values increased as the metal nanoparticles increased, and the values of treated samples in the second method increased more than the first method. Cotton textiles treated with chitosan or NPs have low UV protection (UPF < 20) against UV light, according to their testing. The difference in UPF protection value between cotton fabrics with and without metal nanoparticles is expressed in figure 35.

_____

Egypt. J. Chem. **67,** SI: M. R. Mahran (2024)

Table 1 Effect of metal content (TiO$_2$ NPs, clay NPs and ZnO NPs) inclusion on the UPF values cotton fabrics in the finishing formulation

Metal content & UPF					
Ti (mg/dl)	UPF	Si (mg/dl)	UPF	Zn (mg/dl)	UPF
4	1.25	48.31	7	1.12	4.7	10	1.27	36.5
5	3.19	64.34	8	1.56	7.9	11	3.08	58.2
6	4.56	90.12	9	1.73	8.6	12	4.66	82.8
13	0.63	28.61	16	0.44	3.5	19	0.99	19.5
14	1.77	52.95	17	0.79	4.3	20	2.19	48.02
15	1.96	76.39	18	0.92	4.6	21	3.2	67.93
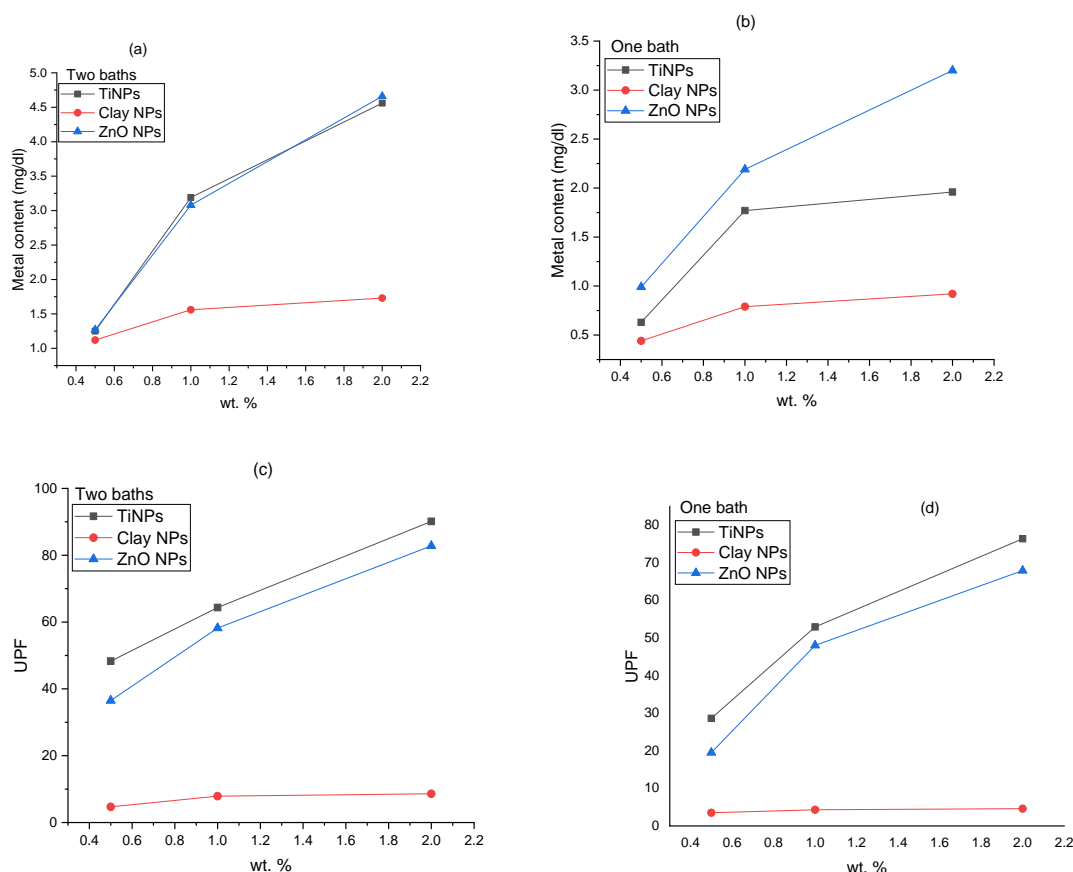
Figure 35. Effect of metal content (TiO2 NPs, clay NPs and ZnO NPs) and UPF values inclusion n the finishing formulation

3.9. Antimicrobial Activity

In this experiment, the samples coded (11, 12, 14, 20, and 21) in group no. 1 and the samples coded (7, 10, and 13) in group no. 2 have excellent antimicrobial activity compared with the other samples. These samples showed an excellent antimicrobial effect on gramme-positive bacteria (Staphylococcus aureus) and pathogenic yeasts (Candida albicans) either using the disc diffusion method to measure the inhibition zone diameter produced by these samples or by applying the shake flask method to calculate the (%) reduction of colony-forming unit (CFU) of the tested strains after

being treated by these sample discs. In addition to the excellent antimicrobial activity of the above samples on gramme-negative bacteria (Escherichia coli), applying the shake flask method to calculate the percentage reduction of colony-forming units (CFU) only with a range of (89.29–96.75%) gives us an indication that these samples have a bacteriostatic effect on gramme-negative bacteria. The excellent antimicrobial activity of the above samples toward both gramme positive pathogenic bacterial strains (Staphylococcus aureus) and pathogenic yeasts (Candida albicans) give us an indication that these samples have a bactericidal and fungicidal effect

toward it with inhibition zone range (18.0-23.0) and (19.0-24.0) for both pathogenic bacterial strains (Staphylococcus aureus) and pathogenic yeasts (Candida albicans) respectively, in addition to their CFU reduction about (85.36 – 99.22 %) and (50.33 – 99.35%) for both pathogenic bacterial strains (Staphylococcus aureus) and pathogenic yeasts (Candida albicans) respectively, also the other samples coded (quatt, 5, 6, 8, 9, 15, 17 & 18) in group no. (1) and the samples coded (Blank, 4, 16 & 19) in group no. (2) were characterized as bacteriostatic agents only toward all pathogenic strains because of their effect on it through reducing the bacterial or fungal population counting of only; therefore, the zone of inhibition, or the circular area surrounding the effective sample where the bacterial colonies don't grow, is measured using the disc diffusion method, which is a more precise and effective antimicrobial method than the total viable count. **[79].**

Table 2: (%) CFU reduction of fabric samples on both bacterial and fungal strains after incubation with the tested samples using the shake flask method

Sample	Reduction percent (%)		
	Escherichi a coli	Staphylococcu s aureus	Candid a albican s
Blank	35.72	27.89	36.65
Quatt	31.52	41.48	25.99
4.0	84.51	61.92	40.87
5.0	41.71	36.31	49.01
6.0	52.67	34.68	53.43
7.0	94.27	86.49	97.28
8.0	76.15	55.99	27.33
9.0	60.73	44.73	49.84
10.0	89.29	92.43	80.67
11.0	96.75	91.58	94.78
12.0	91.73	93.52	92.96
13.0	94.42	85.36	50.33
14.0	94.27	99.22	99.39
15.0	35.33	25.18	0.0
16.0	33.32	21.61	23.85
17.0	46.97	27.31	0.0
18.0	54.88	41.47	36.37
19.0	55.98	75.49	66.50
20.0	90.69	92.14	76.25
21.0	95.63	93.54	99.35

In the disc diffusion method and measuring the zone of inhibition of any sample, the results indicate that this sample has a bactericidal effect on the tested pathogenic strains, so this is the first antimicrobial test to give us the efficacy of our sample used, and from the results that were recorded from it, we can

classify our sample as a bactericidal agent, while if the samples have a bacteriostatic effect, which is determined by the second antimicrobial test: (%) reduction in bacterial or fungal total viable count **[11].**

Table (3): Inhibition zone diameter (millimeter) of of fabric samples:-

Sam ple	Inhibition zone (mm)		
	Escherichi a coli	Staphylococcu s aureus	Candida albicans
7.0	Nil	Nil	Nil
10.0	Nil	21.0	20.0
11.0	Nil	22.0	20.0
12.0	Nil	19.0	21.0
13.0	Nil	Nil	Nil
14.0	Nil	Nil	Nil
20.0	Nil	18.0	19.0
21.0	Nil	23.0	24.0
CN **	18.0	20.0	——— ——
MIZ **	——— ——	——— ——	10

*Nil:- No antimicrobial activity recorded.& ** Reference: CN : Gentamicin 10 mcg (standard antibiotic disc) Bioanalyze &MCZ: Mico 10 mcg (standard antifungal disc) Bioanalyze.

The mode of action of samples coded (11, 12, 14, 20, & 21) in group no. (1) and (7, 10, & 13) in group no. (2) inhibits the bacterial cell wall, which is a mucopolysaccharide component known as peptidoglycan (murein). Gram-positive and Gram-negative bacteria differ in this polymer's amount and position within their cell envelopes **[11].**

Therefore, these samples' effect on bacterial cell walls was caused by the nanostructure of the nanocomposites, which allowed them to enter bacterial and fungal cells and stopped many cascade actions by inhibiting the synthesis of nucleic acids, which in turn inhibited the synthesis of proteins. This was followed by the inhibition of other bacterial metabolism activities, including (i) membrane rupture with inhibition of ATP-ase activity, (ii) leakage of essential biomolecules from the cell, (iii) disruption of the natural motive force, and (iv) enzyme inactivation.[80, 81], from all previous actions lead to the above excellent results on these tested pathogenic strains, Additionally it destroys the budding process by upsetting the structure of the cell membrane and by compromising the integrity of the membrane, which is how it carries out its antifungal action [82, 83].

Finally, the samples coded (11, 12, 14, 20, and 21) in group no. 1 and the samples coded (7, 10, and 13) in group no. 2 have excellent antimicrobial activity toward tested gramme-positive bacteria

(Staphylococcus aureus) and pathogenic yeasts (Candida albicans), respectively, with acts as bactericidal and fungicidal agents. On the other hand, these samples have a reduction only toward gramme-negative bacteria (Escherichia coli), so these samples act as bacteriostatic agents. So from above, these samples showed an excellent effect, so these samples act as promising antimicrobial agents.

3.10. Self-cleaning action of TiO₂NPs loaded fabrics.

The self-cleaning action observed for fabric samples stained with methylene blue (MB) can be attributed to the photocatalytic degradation mechanism of the titanium dioxide and zinc oxide nanoparticles, as illustrated in Figure 36. [9].

Table 4 and Figure 37 present the K/S values for both exposed and unexposed sections of the samples over a 48-hour period. This comparison highlights the self-cleaning efficacy of fabrics treated with TiO2 nanoparticles, clay nanoparticles, and ZnO nanoparticles, utilising either a 1st method or 2nd method treatment approach. The reduction in K/S percentage values for the exposed segment relative to the unexposed sample portion was computed to quantify the self-cleaning effect, indicating the rapid degradation of Methylene Blue stain.

Results showed that all treated fabrics with these nanomaterials have strong self-cleaning properties, and their effect increased as their concentration increased. In addition, the order of self-cleaning action is as follows:

Zinc oxide NPs > Clay NPs>TiO₂ NPs   (1st method)

TiO₂ NPs>ZnO NPs>clay NPs (2nd method)

The generation of reactive oxidation species on the fabric surface forms the foundation for the self-cleaning characteristics observed in cotton fabrics treated with TiO2NPs, clay NPs, and ZnO NPs. When exposed to visible light, the excited methylene blue dye (MB) molecule adsorbed on the fabric's surface donates an electron to the conduction band of TiO₂NPs. Consequently, the reactive oxidation species, formed by the electron captured by molecular oxygen on the nanoparticles' surface, catalyzes the photocatalytic degradation of the MB stain, as follows:
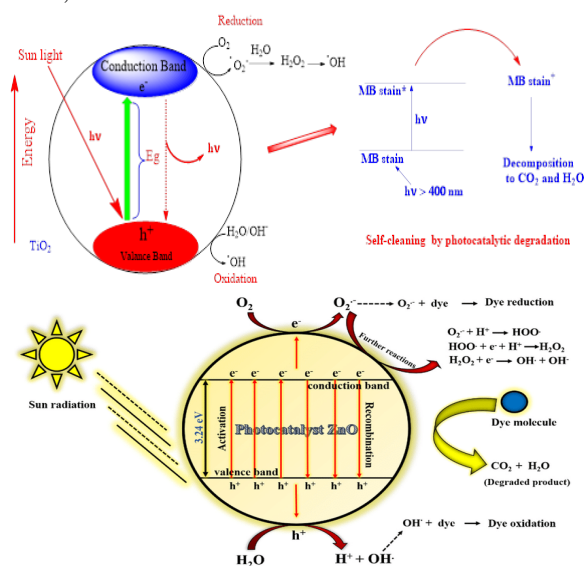
Figure 36: TiO₂ NPs and ZnO photocatalytic degradation and photoexcitation lead to the production of reactive oxidation species and the self-cleaning of MB stain.[9]

In this context, the selection of TiO₂, clay, and ZnO nanoparticles influencing the discoloration of Methylene Blue (MB) is contingent upon the presence of these nanoparticles. This phenomenon is ascribed to the heightened band gap of nanoparticle irradiation. The excitation of electrons from the valence band to the conduction band creates positive holes (h+). Both electrons (e') in the conduction band and positive holes (h+) in the valence band instigate reduction and oxidation reactions, respectively. Consequently, reactive oxygen species such as O2. and OH. are formed, capable of interacting with deleterious organic materials and decomposing them into less harmful byproducts. [84].

MB stain + reactive Oxygen species (OH, $\overset{\bullet}{O}$H₂, H₂$\overset{\bullet}{O}$₂, etc) ⟶ Photocatalytic degradation products

Table 4. Percentage decrease in K/S of MB-degradation on exposure to sunlight

Self-cleaning											
TiO₂ NPs				Clay NPs				ZnO NPs			
S	(K/S)a	(K/S)b	Discoloration (%)	S	(K/S)a	(K/S)b	Discoloration (%)	S	(K/S)a	(K/S)b	Discoloration (%)
4	0.65	0.92	70.65	7	0.4	0.55	72.73	10	0.64	0.45	70.31
5	0.86	0.75	87.21	8	0.51	0.44	86.27	11	0.5	0.45	90.00
6	0.7	0.76	92.11	9	0.57	0.58	98.28	12	0.48	0.48	100.00
13	0.49	0.82	59.61	16	0.35	0.6	58.33	19	0.46	0.6	76.67
14	0.5	0.7	71.43	17	0.39	0.58	67.24	20	0.53	0.68	77.95
15	0.87	0.97	89.69	18	0.4	0.57	70.18	21	0.53	0.63	84.13
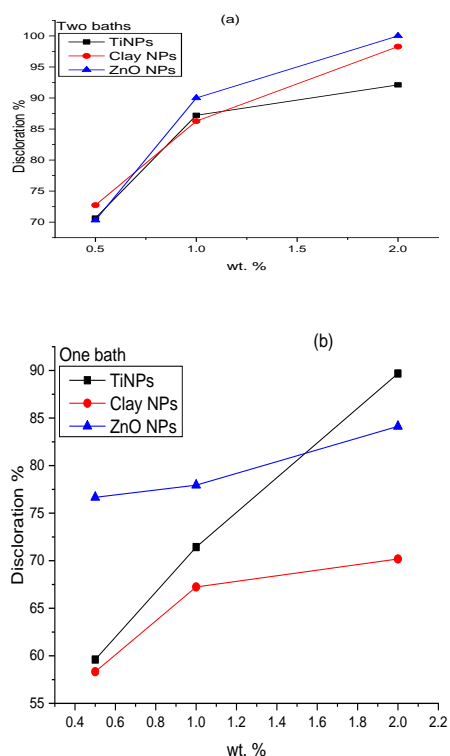
Figure 37. Self-cleaning effect of TiO$_2$ NPs, clay NPs and ZnO NPs expressed in discoloration of MD at 1st &2nd method treatment of modified cotton fabrics with nanoparticles

4. Conclusion

The application of natural biopolymers and inorganic nanoparticles holds immense potential for functionalizing textile fabrics with diverse and valuable properties. Chitosan/quatt188, along with clay, ZnO, and TiO2 nanoparticles, emerge as effective materials for achieving multifunctional coatings with antimicrobial, UV blocking, stain repellent, and flame-retardant capabilities. The use of these materials, coupled with efficient coating techniques, paves the way for developing sustainable and high-performance textiles with enhanced functionality for diverse applications. Further research and innovation in this domain are crucial to unlocking the full potential of this technology and creating next-generation textiles that cater to evolving needs in various sectors. The extent of the reaction between cotton fabric and 1- CS/NPs solo or for/2- cotton fabric treated first with quatt188/Cs/NPs depends on the reaction sequence and reaction parameters. The latter include the reaction temperature and reaction time as well as the alkali and reactant concentration i.e application of optimum conditions for cationization treatment . A greater reaction was attained when the cotton fabric was first cationized with Quat-188, then allowed to react with Cs/NPs in the absence of alkali. The

cationic groups in the precationized cotton fabric form an alkali site that might stimulate in-situ the reaction between composite and pre-cationized cotton. A lower modification was obtained when the reaction was carried out in one step[1st method].

6. Conflict of interest

The authors have no conflict of interest

8. References:

[1]. W.A. Daoud, J.H. Xin, Low temperature sol-gel processed photocatalytic titania coating, Journal of Sol-Gel Science and Technology 29 (2004) 25-29.

[2]. N. Ghasemi, M. Ghasemi, S. Moazeni, P. Ghasemi, N.S. Alharbi, V.K. Gupta, S. Agarwal, I.V. Burakova, A.G. Tkachev, Zn (ii) removal by amino-functionalized magnetic nanoparticles: Kinetics, isotherm, and thermodynamic aspects of adsorption, Journal of industrial and engineering chemistry 62 (2018) 302-310.

[3]. A.P. Periyasamy, M. Venkataraman, D. Kremenakova, J. Militky, Y. Zhou, Progress in sol-gel technology for the coatings of fabrics, Materials 13(8) (2020) 1838.

[4]. B.M. Kale, J. Wiener, J. Militky, S. Rwawiire, R. Mishra, K.I. Jacob, Y. Wang, Coating of cellulose-tio2 nanoparticles on cotton fabric for durable photocatalytic self-cleaning and stiffness, Carbohydr. Polym. 150 (2016) 107-113.

[5]. B. Mahltig, D. Fiedler, H. Böttcher, Antimicrobial sol–gel coatings, Journal of sol-gel science and technology 32 (2004) 219-222.

[6]. N. Vigneshwaran, S. Kumar, A.A. Kathe, P.V. Varadarajan, V. Prasad, Functional finishing of cotton fabrics using zinc oxide–soluble starch nanocomposites, Nanotechnology 17(20) (2006) 5087.

[7]. A. Kołodziejczak-Radzimska, T. Jesionowski, Zinc oxide—from synthesis to application: A review, Materials 7(4) (2014) 2833-2881.

[8]. S. Farag, A. Amr, A. El-Shafei, M.S. Asker, H.M. Ibrahim, Green synthesis of titanium dioxide nanoparticles via bacterial cellulose (bc) produced from agricultural wastes, Cellulose 28(12) (2021) 7619-7632.

_____

[9]. I. Moussa, H. Ibrahim, E.A.M. Emam, T.M. Tawfik, Structure, light absorption properties and photocatalytic activity of carbon-containing titania nanocomposites synthesized via a facile sol–gel method, Heliyon 8(8) (2022).

[10]. E. Pakdel, W.A. Daoud, Self-cleaning cotton functionalized with tio2/sio2: Focus on the role of silica, J. Colloid Interface Sci. 401 (2013) 1-7.

[11]. S. Farag, H.M. Ibrahim, M.S. Asker, A. Amr, A. El-Shafaee, Impregnation of silver nanoparticles into bacterial cellulose: Green synthesis and cytotoxicity, International Journal of ChemTech Research 8(12) (2015) 651-661.

[12]. R. Farouk, Y.A. Youssef, A.A. Mousa, H.M. Ibrahim, Simultaneous dyeing and antibacterial finishing of nylon 6 fabric using reactive cationic dyes, World Applied Sciences Journal 26(10) (2013) 1280-1287.

[13]. R.G. Nawalakhe, S.M. Hudso, A.M. Seyam, A.I. Waly, N.Y. Abou-Zeid, H.M. Ibrahim, Development of electrospun iminochitosan for improved wound healing application, Journal of Engineered Fibers and Fabrics 7(2) (2012) 47-55.

[14]. W.A.I. Al-Megrin, M.F. El-Khadragy, F.A. Mohamed, H.M. Ibrahim, Free salt dyeing by treatment of cotton fabric using carboxyethyl chitosan and synthesized direct dyes to enhance dyeing properties and antibacterial activity, Current Organic Synthesis 20(8) (2023) 910-918.

[15]. R. Salama, H. Osman, H.M. Ibrahim, Preparation of biocompatible chitosan nanoparticles loaded with aloe vera extract for use as a novel drug delivery mechanism to improve the antibacterial characteristics of cellulose-based fabrics, Egypt. J. Chem. 65(3) (2022) 581-595.

[16]. R.M. Mosaad, M.H. Alhalafi, E.A.M. Emam, M.A. Ibrahim, H. Ibrahim, Enhancement of antimicrobial and dyeing properties of cellulosic fabrics via chitosan nanoparticles, Polymers 14(19) (2022).

[17]. A. Yadav, V. Prasad, A.A. Kathe, S. Raj, D. Yadav, C. Sundaramoorthy, N. Vigneshwaran, Functional finishing in cotton fabrics using zinc oxide nanoparticles, Bulletin of materials Science 29 (2006) 641-645.

[18]. M. Joshi, A. Bhattacharyya, Nanotechnology–a new route to high-performance functional textiles, Textile progress 43(3) (2011) 155-233.

[19]. N. Vrinceanu, S. Bucur, C.M. Rimbu, S. Neculai-Valeanu, S. Ferrandiz Bou, M.P. Suchea, Nanoparticle/biopolymer-based coatings for functionalization of textiles: Recent developments (a minireview), Textile Research Journal 92(19-20) (2022) 3889-3902.

[20]. M.M. El-Zawahry, A.G. Hassabo, F. Abdelghaffar, R.A. Abdelghaffar, O.A. Hakeim, Preparation and use of aqueous solutions magnetic chitosan / nanocellulose aerogels for the sorption of reactive black 5, Biointerf. Res. Appl. Chem. 11(4) (2021) 12380 - 12402.

[21]. A. Yasser, H. Mahmoud, M. Said, R. Aymen, Y. Ashraf, A.I. Fathallah, D. Maamoun, M.S. Abdelrahman, A.G. Hassabo, T.A. Khattab, Multifunctional properties of cotton fabric treated with chitosan and rtv silicone, J. Text. Color. Polym. Sci. 20(1) (2023) 125-130.

[22]. A.G. Hassabo, A.L. Mohamed, Multiamine modified chitosan for removal metal ions from their aqueous solution BioTechnology: An Indian Journal 12(2) (2016) 59-69.

[23]. M.M. El-Zawahry, F. Abdelghaffar, R.A. Abdelghaffar, A.G. Hassabo, Equilibrium and kinetic models on the adsorption of reactive black 5 from aqueous solution using eichhornia crassipes/chitosan composite, Carbohydrate Polymers 136 (2016) 507-515.

[24]. A. Hebeish, S. Shaarawy, A.G. Hassabo, A. El-Shafei, Eco-friendly multifinishing of cotton through inclusion of motmorillonite/chitosan hybrid nanocomposite, Der Phar. Chem. 8(20) (2016) 259-271.

[25]. W. Guo, H. Hao, S. Jin, Q. Su, H. Li, X. Hu, Y. Gan, L. Qin, W. Gao, G. Liu, Preparation and infrared to visible upconversion luminescence of yb2o3: Ho3+ nanocrystalline powders, Ceramics International 43(5) (2017) 4330-4334.

[26]. M.P. Sathianarayanan, N.V. Bhat, S.S. Kokate, V.E. Walunj, Antibacterial finish for cotton fabric from herbal products, (2010).

[27]. B.M. Hegazy, H. Othman, A.G. Hassabo, Polycation natural materials for improving textile dyeability and functional performance, J. Text. Color. Polym. Sci. 19(2) (2022) 155-178.

[28]. A.G. Hassabo, E. Reda, H. Ghazal, H. Othman, Enhancing printability of natural fabrics via pre-treatment with polycationic polymers, Egy. J. Chem. 66(2) (2023) 167-181.

[29]. ASTM Standard Test Method (D5035-2011 (Reapproved 2019)), Standard test method for breaking force and elongation of textile fabrics (strip method), ASTM International, 2019.

[30]. A.G. Hassabo, M.M. Ragab, H.A. Othman, Ultraviolet protection of cellulosic fabric, J. Text. Color. Polym. Sci. 19(1) (2022) 51-61.

[31]. A.G. Hassabo, M. Salama, A.L. Mohamed, C. Popescu, Ultrafine wool and cotton powder and their characteristics, J. Nat. Fiber 12(2) (2015) 141-153.

[32]. M. Zayed, H. Ghazal, H. Othman, A.G. Hassabo, Psidium guajava leave extract for improving ultraviolet protection and antibacterial properties of cellulosic fabrics, Biointerf. Res. Appl. Chem. 12(3) (2022) 3811 - 3835.

[33]. N.S. Elshemy, A.G. Hassabo, Z.M. Mahmoud, K. Haggag, Novel synthesis of nano-emulsion butyl methacrylate/acrylic acid via micro-emulsion polymerization and ultrasonic waves, JTATM 10(1) (2016) 1-16.

[34]. M.S. Kamal, E. Mahmoud, A.G. Hassabo, M.M. Eid, Effect of some construction factors of bi-layer knitted fabrics produced for sports wear on resisting ultraviolet radiation, Egy. J. Chem. 63(11) (2020) 4369 - 4378.

[35]. A.G. Hassabo, M. Salama, C. Popescu, Characterizations of pva composites based on recycled ultrafine cotton and wool powders, Res. Rev. BioSci. 10(14) (2015) 147-158.

[36]. H. Ibrahim, E.A.M. Emam, T.M. Tawfik, A.T. El-Aref, Preparation of cotton gauze coated with carboxymethyl chitosan and its utilization for water filtration, J. Text. Appar. Technol. Manag. 11(1) (2019).

[37]. A.G. Hassabo, A.L. Mohamed, Novel flame retardant and antibacterial agent containing mgo nps, phosphorus, nitrogen and silicon units for functionalise cotton fabrics, Biointerf. Res. Appl. Chem. 9(5) (2019) 4272 - 4278.

[38]. A.L. Mohamed, A.G. Hassabo, Engineered carbohydrate based material/silane as a thermo and ph-sensitive nanogel containing zinc oxide nanoparticles for antibacterial textile, International Conference on Medical Textiles and Healthcare Products (MedTex 2015), Department of Material and Commodity Sciences and Textile Metrology, Faculty of Material Technologies and Textile Design, Lodz University of Technology, Lodz, Poland, 2015.

[39]. A.L. Mohamed, A.G. Hassabo, Composite material based on pullulan/silane/zno-nps as ph, thermo-sensitive and antibacterial agent for cellulosic fabrics, Adv. Nat. Sci.: Nanosci. Nanotechnol. 9(4) (2018) 045005 (1-9).

[40]. A.L. Mohamed, A.G. Hassabo, Cellulosic fabric treated with hyperbranched polyethyleneimine derivatives for improving antibacterial, dyeing, ph and thermo-responsive performance, Int. J. Biol. Macromol. 170 (2021) 479-489.

[41]. A.L. Mohamed, A.G. Hassabo, S. Shaarawy, A. Hebeish, Benign development of cotton with antibacterial activity and metal sorpability through introduction amino triazole moieties and agnps in cotton structure pre-treated with periodate, Carbohydrate Polymers 178 (2017) 251-259.

[42]. E.F. Attia, T.W. Helal, L.M. Fahmy, M.A. Wahib, M.M. Saad, S. Abd El-Salam, D. Maamoun, S.A. Mahmoud, A.G. Hassabo, T.A. Khattab, Antibacterial, self-cleaning, uv protection and water repellent finishing of polyester fabric for children wheelchair, J. Text. Color. Polym. Sci. 20(2) (2023) 181-188.

[43]. A.G. Hassabo, S. Ebrahim, H.A. Othman, M.M. Mosaad, Using pectin to enhance the dyeability performance and antimicrobial activity using different dyes on modified proteinic and synthetic fabrics, Biointerf. Res. Appl. Chem. 13(5) (2023) BRIAC135.467.

[44]. N.A. Ibrahim, A.A. Nada, A.G. Hassabo, B.M. Eid, A.M. Noor El-Deen, N.Y. Abou-Zeid, Effect of different capping agents on physicochemical and antimicrobial properties of zno nanoparticles, Chem. Pap. 71(7) (2017) 1365-1375.

[45]. Z.S. Gaafar, Y.A.E.-m. Roshdy, M.N. El-Shamy, H.A. Mohamed, A.G. Hassabo, Antimicrobial processing techniques for fabric enhancement, J. Text. Color. Polym. Sci. (2024) -.

[46]. M. Mahmoud, N. Sherif, A.I. Fathallah, D. Maamoun, M.S. Abdelrahman, A.G. Hassabo, T.A. Khattab, Antimicrobial and self-cleaning finishing of cotton fabric using titanium dioxide nanoparticles, J. Text. Color. Polym. Sci. 20(2) (2023) 197-202.

[47]. A. Ehab, A. Mostafa, E. Mohamed, E. Magdi, R. Mossad, D. Maamoun, H. Khalil, H. El-Hennawy, A.G. Hassabo, T.A. Khattab, Antimicrobial and blood-repellent finishes of surgical gowns, J. Text. Color. Polym. Sci. 20(1) (2023) 131-135.

[48]. K.A. Abdel Salam, N.A. Ibrahim, D. Maamoun, S.H. Abdel Salam, A.I. Fathallah, M.S. Abdelrahman, H. Mashaly, A.G. Hassabo, T.A. Khattab, Anti-microbial finishing of polyamide fabric using titanium dioxide nanoparticles, J. Text. Color. Polym. Sci. 20(2) (2023) 171-174.

[49]. M.Y. Kamel, A.G. Hassabo, Anti-microbial finishing for natural textile fabrics, J. Text. Color. Polym. Sci. 18(2) (2021) 83-95.

[50]. M.N. El-Shamy, H.A. Mohamed, Z.S. Gaafar, Y.A.E.-m. Roshdy, A.G. Hassabo, Advancements in bioactive textiles: A review of antimicrobial fabric finishes and commercial products, J. Text. Color. Polym. Sci. (2024) -.

[51]. N.A. Ibrahim, A. Amr, B.M. Eid, A.A. Almetwally, M.M. Mourad, Functional finishes of stretch cotton fabrics, Carbohydrate Polymers 98(2) (2013) 1603-1609.

[52]. M. Diaa, A.G. Hassabo, Self-cleaning properties of cellulosic fabrics (a review), Biointerf. Res. Appl. Chem. 12(2) (2022) 1847 - 1855.

[53]. S. S., S. A., S. A., A. S., D. Maamoun, A.G. Hassabo, S.A. Mahmoud, T.A. Khattab, Self-cleaning finishing of polyester fabrics using znonps, J. Text. Color. Polym. Sci. 21(1) (2024) 103-107.

[54]. Y.A.E.-m. Roshdy, M.N. El-Shamy, H.A. Mohamed, Z.S. Gaafar, A.G. Hassabo, Self-cleaning cotton textiles enhanced with nanotechnology, J. Text. Color. Polym. Sci. (2024) -.

[55]. M. Adel, M. Mohamed, M. Mourad, M. Shafik, A. Fathallah, D. Maamoun, M.S. Abdelrahman, A.G. Hassabo, T.A. Khattab, Enhancing the self-cleaning properties of polyester fabric with rtv – silicone rubber, J. Text. Color. Polym. Sci. 21(1) (2024) 91-95.

[56]. D. Tarek, A. Mohmoud, Z. Essam, R. Sayed, A. Maher, D. Maamoun, S.H. Abdel Salam, H. Mohamed, A.G. Hassabo, T.A. Khattab, Development of wrinkle free and self-cleaning finishing of cotton and polyester fabrics, J. Text. Color. Polym. Sci. 20(2) (2023) 175-180.

[57]. F. Tomczak, K.G. Satyanarayana, T.H.D. Sydenstricker, Studies on lignocellulosic fibers of brazil: Part iii–morphology and properties of brazilian curauá fibers, Composites Part A: Applied Science and Manufacturing 38(10) (2007) 2227-2236.

[58]. P. Khalili, K.Y. Tshai, D. Hui, I. Kong, Synergistic of ammonium polyphosphate and alumina trihydrate as fire retardants for natural fiber reinforced epoxy composite, Composites Part B: Engineering 114 (2017) 101-110.

[59]. I.M. De Rosa, J.M. Kenny, D. Puglia, C. Santulli, F. Sarasini, Morphological, thermal and mechanical characterization of okra (abelmoschus esculentus) fibres as potential reinforcement in polymer composites, Composites Science and Technology 70(1) (2010) 116-122.

[60]. R.H. Daiane, O.J. Luiz, C.A. Sandro, J.Z. Ademir, Preparation and characterization of ramie-glass fibre reinforced polymer matrix hybrid composite, Engeharia de material Rod 4(7) (2011) 445-452.

[61]. N. Sgriccia, M.C. Hawley, M. Misra, Characterization of natural fiber surfaces and natural fiber composites, Composites Part A:

Applied Science and Manufacturing 39(10) (2008) 1632-1637.

[62]. A. Tarbuk, A.M. Grancaric, M. Leskovac, Novel cotton cellulose by cationisation during the mercerisation process—part 1: Chemical and morphological changes, Cellulose 21(3) (2014) 2167-2179.

[63]. Y. Yue, G. Han, Q. Wu, Transitional properties of cotton fibers from cellulose i to cellulose ii structure, BioResources 8(4) (2013) 6460-6471.

[64]. R. Brandes, L. de Souza, V. Vargas, E. Oliveira, A. Mikowski, C. Carminatti, H. Al-Qureshi, D. Recouvreux, Preparation and characterization of bacterial cellulose/tio2 hydrogel nanocomposite, Journal of Nano Research, Trans Tech Publ, 2016, pp. 73-80.

[65]. D. Sun, J. Yang, X. Wang, Bacterial cellulose/tio2 hybrid nanofibers prepared by the surface hydrolysis method with molecular precision, Nanoscale 2(2) (2010) 287-292.

[66]. L. Yang, C. Chen, Y. Hu, F. Wei, J. Cui, Y. Zhao, X. Xu, X. Chen, D. Sun, Three-dimensional bacterial cellulose/polydopamine/tio2 nanocomposite membrane with enhanced adsorption and photocatalytic degradation for dyes under ultraviolet-visible irradiation, J. Colloid Interface Sci. 562 (2020) 21-28.

[67]. S. Bagheri, K. Shameli, S.B. Abd Hamid, Synthesis and characterization of anatase titanium dioxide nanoparticles using egg white solution via sol-gel method, Journal of Chemistry 2013 (2013) 848205.

[68]. N. Abidi, L. Cabrales, E. Hequet, Functionalization of a cotton fabric surface with titania nanosols: Applications for self-cleaning and uv-protection properties, Acs Appl. Mater. Inter. 1(10) (2009) 2141-2146.

[69]. A. Khalid, H. Ullah, M. Ul-Islam, R. Khan, S. Khan, F. Ahmad, T. Khan, F. Wahid, Bacterial cellulose–tio2 nanocomposites promote healing and tissue regeneration in burn mice model, RSC Adv. 7(75) (2017) 47662-47668.

[70]. I. Uysal, F. Severcan, Z. Evis, Characterization by fourier transform infrared spectroscopy of hydroxyapatite co-doped with zinc and fluoride, Ceramics International 39(7) (2013) 7727-7733.

[71]. A. Arputharaj, V. Nadanathangam, S.R. Shukla, A simple and efficient protocol to develop durable multifunctional property to cellulosic materials using in situ generated nano-zno, Cellulose 24 (2017) 3399-3410.

[72]. M.G. Al-Khuzaie, S.M. Al-Majidi, Synthesis and characterization of new azo compounds linked to 1, 8-naphthalimide as new fluorescent dispersed dyes for cotton fibers, Journal of Physics: Conference Series, IOP Publishing, 2020, p. 012065.

[73]. H. Zheng, Y. Zhong, Z. Mao, L. Zheng, Co2 utilization for the waterless dyeing: Characterization and properties of disperse red 167 in supercritical fluid, J. CO2 Util. 24 (2018) 266-273.

[74]. M. Montazer, A. Behzadnia, E. Pakdel, M.K. Rahimi, M.B. Moghadam, Photo induced silver on nano titanium dioxide as an enhanced antimicrobial agent for wool, Journal of Photochemistry and Photobiology B: Biology 103(3) (2011) 207-214.

[75]. W. Li, R. Liang, A. Hu, Z. Huang, Y.N. Zhou, Generation of oxygen vacancies in visible light activated one-dimensional iodine tio 2 photocatalysts, RSC advances 4(70) (2014) 36959-36966.

[76]. D. Sridev, K.V. Rajendran, Synthesis and optical characteristics of zno nanocrystals, Bulletin of Materials Science 32 (2009) 165-168.

[77]. J. Golebiewski, A. Rozanski, J. Dzwonkowski, A. Galeski, Low density polyethylene–montmorillonite nanocomposites for film blowing, European Polymer Journal 44(2) (2008) 270-286.

[78]. N.A. Ibrahim, B.M. Eid, M.S. Abdel-Aziz, Green synthesis of aunps for eco-friendly functionalization of cellulosic substrates, Applied Surface Science 389 (2016) 118-125.

[79]. M.A. Ali, E.A. Bydoon, H.M. Ibrahim, Bioactive composite nonwoven surgical dressing based on cellulose coated with nanofiber membrane using the layer-by-layer technique, Egypt. J. Chem. 65(4) (2022) 525-542.

[80]. H.M. Ibrahim, M.K. El-Bisi, G.M. Taha, E.A. El-Alfy, Chitosan nanoparticles loaded antibiotics as drug delivery biomaterial, Journal of Applied Pharmaceutical Science 5(10) (2015) 85-90.

[81]. M.K. El-Bisi, H.M. Ibrahim, A.M. Rabie, K. Elnagar, G.M. Taha, E.A. El-Alfy, Super hydrophobic cotton fabrics via green techniques, Der Pharma Chemica 8(19) (2016) 57-69.

[82]. H.M. Ibrahim, E.M.R. El-Zairy, Carboxymethylchitosan nanofibers containing silver nanoparticles: Preparation, characterization and antibacterial activity, Journal of Applied Pharmaceutical Science 6(7) (2016) 43-48.

[83]. E.A. El-Alfy, M.K. El-Bisi, G.M. Taha, H.M. Ibrahim, Preparation of biocompatible chitosan nanoparticles loaded by tetracycline, gentamycin and ciprofloxacin as novel drug delivery system for improvement the antibacterial properties of cellulose based fabrics, Int. J. Biol. Macromol. 161 (2020) 1247-1260.

[84]. D. Wu, M. Long, J. Zhou, W. Cai, X. Zhu, C. Chen, Y. Wu, Synthesis and characterization of self-cleaning cotton fabrics modified by tio2 through a facile approach, Surface and Coatings Technology 203(24) (2009) 3728-3733.